

Temporal Gating for the Optimization of Laser-Induced Breakdown Spectroscopy Detection and Analysis of Toxic Metals

BRIAN T. FISHER, HOWARD A. JOHNSEN, STEVEN G. BUCKLEY, and DAVID W. HAHN*

Department of Mechanical Engineering, University of Florida, Gainesville, Florida 32611-6300 (B.T.F., D.W.H.); Sandia National Laboratories, Livermore, California 94551-0969 (H.A.J.); and Department of Mechanical Engineering, University of Maryland, College Park, Maryland 20742 (S.G.B.)

Optimal temporal gating for laser-induced breakdown spectroscopy (LIBS) analysis was investigated for a select group of toxic metals, namely the Resource Conservation and Recovery Act (RCRA) metals arsenic, beryllium, cadmium, chromium, lead, and mercury. The differing rates of decay between the continuum plasma emission and the atomic emission were used as a means to maximize the signal-to-noise ratio of the atomic emission lines for these six metal species. Detection windows were investigated corresponding to delay times from 2 to 50 μs following the plasma-initiating laser pulse. For the current experimental conditions, it is concluded that the relatively short delay time of 12 μs is optimal for the detection of arsenic, beryllium, cadmium, and mercury, while a longer delay time of 50 μs is optimal for the detection of chromium and lead. The reduced atomic emission intensity at relatively long delay times is compensated for by the use of long detector gate widths. Estimated detection limits are reported for the six metal species based on the optimized temporal gating and ensemble averaging of multiple laser pulses, and the implications for simultaneous metals monitoring are discussed.

Index Headings: Laser-induced breakdown spectroscopy (LIBS); Laser-induced plasma spectroscopy; Metal emissions.

INTRODUCTION

In recent years there has been an increased awareness of and public interest in the health risks associated with toxic metals, specifically, smokestack emissions from industrial furnaces and hazardous waste incinerators, as well as the concentration levels of toxic metal species in ambient air. In particular, urban areas may be subject to additional public health risks resulting from a larger concentration of stationary and mobile emission sources. Enhanced awareness by the general public has provided scientists, engineers, and health professionals with a unique opportunity to make an impact in these important research areas. Specific research needs to include ambient air monitoring and monitoring of smokestack emissions, analyses to characterize the sources of ambient air toxics, and considerations of atmospheric transformation processes associated with these metal-based toxics. Experimental data regarding these items form the cornerstone for many other targeted research areas, including evaluation of exposure levels and estimates of risk, emission reduction strategies, and modeling efforts.

Recent maximum achievable control technology (MACT) standards for hazardous waste emissions from

boilers and industrial furnaces encourage the development and use of continuous emissions monitors, notably for toxic metal-based species.¹ In response to these needs, several real-time emissions monitors have been developed for metal-based toxics emissions, incorporating technologies such as inductively coupled plasma atomic emission spectroscopy (ICP-AES), microwave-induced plasma atomic emission spectroscopy (MIP-AES), and laser-induced breakdown spectroscopy (LIBS).²⁻⁴ One technology, based on ICP-AES, has been developed commercially by Thermo Elemental Corporation for the detection of multiple metal species, as reported recently.⁵ LIBS has also been deployed as a real-time metals monitor on thermal waste treatment processes.⁶⁻⁹ Mercury, in particular, because of its widespread use, high degree of toxicity, and high volatility with respect to other toxic metals, has received considerable attention, with a number of analytical techniques for mercury detection reviewed recently.¹⁰

The present paper will focus on laser-induced breakdown spectroscopy for the detection and monitoring of hazardous air pollutant metals, specifically, the elements arsenic, beryllium, cadmium, chromium, lead, and mercury. These six elements are listed by the Resource Conservation and Recovery Act (RCRA) as metals that have been designated by the U.S. Environmental Protection Agency as the primary metals of interest for the development of advanced continuous emissions monitoring technologies. LIBS is an atomic emission spectroscopy diagnostic technique that uses a high-power pulsed laser beam as the excitation source to produce an optical breakdown of the surrounding gas. The resulting optical breakdown, also referred to as a laser-induced plasma or laser spark, exhibits temperatures as high as 15 000 to 20 000 K, atomizing species, and subsequently exciting free atoms within the ensuing microplasma volume. The resulting continuum emission and the discrete atomic emission, both neutral (I) and ionic (II) lines, decay with time, but persist strongly on the order of tens of microseconds. The temporal characteristics are coupled to the sensitivity of the LIBS technique to various analyte species. Temporal optimization of the plasma decay process for the analysis of RCRA-listed toxic metals is the focus of this paper.

Temporal Gating—Background. The LIBS technique has been applied specifically to the detection of elemental species in gaseous media, including several studies that focused on toxic metal compounds. Although

Received 12 March 2001; accepted 10 June 2001.
* Author to whom correspondence should be sent.

no research to date has focused primarily on the temporal characteristics of LIBS emission for the six toxic metals evaluated in this study, nearly all relevant studies make use of time gating to enhance the atomic lines of the LIBS spectra. This is due to the differing rates of decay between the continuum emission and atomic emission. Radziemski et al. performed a detailed analysis of beryllium detection with LIBS by using a temporal integration between 1 and 20 μs with respect to the incident laser pulse.¹¹ The authors noted that local thermodynamic equilibrium was realized in the plasma at times greater than 1 μs for a laser pulse energy of 300 mJ. Cadmium, lead, and zinc were detected with the use of LIBS with a detector gate width of 1 μs and delay times ranging from 20 to 40 μs .¹² The corresponding plasma temperature, based on the two-line Boltzmann method, varied between 5500 and 6500 K at the relevant delay times. Casini et al. discussed the use of time-resolved LIBS for quantitative evaluation of air pollutants.¹³ They noted the importance of optimizing the time delay for signal integration, but provided no specific data. Lazzari et al. focused on mercury detection with the use of LIBS and reported a detection limit of 5 parts per billion (ppb).¹⁴ The signal-to-noise ratio was optimized for their parameters (400 mJ pulse laser) by using a detector gate of 3.5 μs , with a delay time of 15 μs . They also noted that larger delay times would improve the line/continuum intensity ratio, but that the absolute emission intensity can be too low for efficient detection. Schechter used LIBS for the direct analysis of aerosols, including lead and zinc.¹⁵ Detector delay and integration times were optimized for the best signal-to-noise ratios, but no specific gating parameters were provided.

Several studies that used LIBS for the analysis of metallic species were conducted in practical environments and industrial processes. Flower et al. studied the application of LIBS for the analysis of chromium emissions associated with electroplating processes.¹⁶ Zhang et al. studied LIBS-based analysis in both a laboratory methane/air flame and a coal-fired magnetohydrodynamic facility.¹⁷ Calcium, aluminum, barium, manganese, magnesium, iron, strontium, and titanium were detected with the use of a time delay of 1 μs and a detector gate width of 3 μs . Hahn et al. used LIBS for the quantitative measurement of chromium, manganese, and iron concentrations in a pyrolytic waste processing facility with the use of a time delay of 6 μs and a detector gate width of 3.5 μs .⁶ Good agreement was obtained between LIBS-based metals concentration data and independent extractive sampling concentration data. LIBS was evaluated as a process monitoring and control tool for the analysis of toxic metals during hazardous waste remediation in a plasma torch facility.¹⁸ The same research group recently reported LIBS-based measurements of beryllium, cadmium, chromium, and lead in a pilot-scale rotary kiln incinerator.⁷ A time-gated detector was used for plasma emission integration, although no data was provided as to the specific values. *In situ* LIBS measurements were in good agreement with independent extractive sampling data for a range of metal concentrations. Singh et al. also investigated the effects of atmospheric conditions on the LIBS-based analysis of metal hydrides, namely, arsenic and tin.¹⁹ The signal-to-noise was maximized by using a

time delay of 5 μs and a detector integration time from 10 to 20 μs . Yalcin et al. assessed the sensitivity of the LIBS technique to ambient conditions (e.g., gas composition, the presence of particles, relative humidity, and laser power) with an emphasis on the application of toxic metals monitoring.²⁰ The plasma was found to be remarkably robust, as measured by plasma temperature and free electron density, with respect to the ambient conditions over a range of 40 to 150 mJ per laser pulse. Their study, however, was limited to the temporal region between 0.2 and 2 μs after the laser pulse. Neuhauser et al. used LIBS for the detection of lead aerosols.²¹ They reported an optimum signal-to-noise ratio with the use of an integration time of 20 to 50 μs for a laser pulse energy of 45 mJ and noted that the plasma emission was no longer observed after a delay time of 70 μs . Hahn used LIBS for the detection and analysis of individual aerosol particles that contain iron and magnesium by using detection delay times that ranged from 3.5 to 14 μs and signal integration times from 6 to 14 μs .²² A more recent study focused on calcium, chromium, and magnesium based aerosol detection with the use of a delay time of 50 μs and an integration time of 150 μs .²³

As discussed above, a number of studies have utilized LIBS for the analysis of metallic species. Temporal gating of the emission signal is generally used to enhance signal-to-noise ratios by recognizing that different decay rates characterize the continuum emission and atomic emission processes. Spectral interference may also be minimized by taking advantage of the differing relaxation times between different elements.²⁴ The majority of relevant LIBS studies have explored a temporal region that begins several microseconds after the plasma-initiating laser pulse (i.e., after the onset of local thermodynamic equilibrium) and lasts for 10 to 20 microseconds. This temporal region can provide pronounced plasma intensity levels, both continuum and atomic emission, but may also be characterized by significant levels of signal noise. The goal of this paper is to systematically explore temporal signal gating of the LIBS technique for the optimal detection and analysis of the RCRA-listed metals As, Be, Cd, Cr, Hg, and Pb. Specific attention is given to the use of very long detector delay and integration times (50 and 150 μs , respectively), which have often been overlooked in previous studies.

EXPERIMENTAL METHODS

A Q-switched Nd:YAG laser ($\lambda = 1064 \text{ nm}$) was used as the excitation source for all experiments, operating with a nominal pulse width of 10 ns and 5 Hz pulse repetition rate. A schematic of the experimental LIBS setup is shown in Fig. 1. The beam was expanded to 12 mm by using a telescope (not shown schematically), passed through a 50 mm diameter pierced mirror, and then focused with a 75-mm-focal-length, 50 mm diameter UV grade lens to create the plasma. The 50 mm diameter focusing lens also functioned to collect and collimate the plasma emission. The collimated plasma emission was diverted from the beam path with the use of the pierced mirror, launched into a fiber-optic bundle by using a matched 75-mm-focal-length lens, and coupled to a 0.25 m spectrometer (2400 groove/mm). The plasma emission

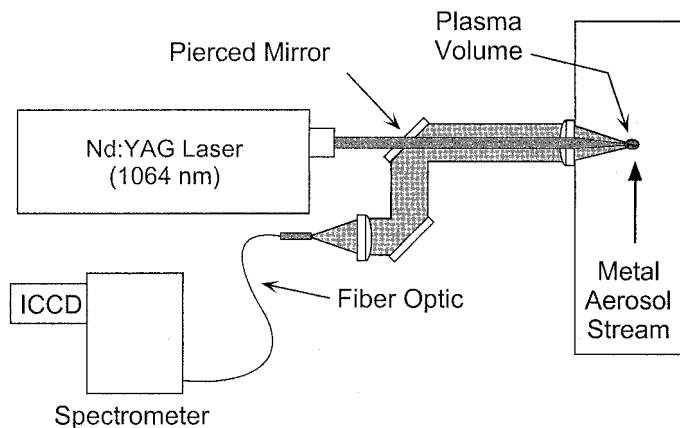


FIG. 1. Schematic diagram of the LIBS configuration.

was recorded with the use of a time-gated, intensified charge-coupled device (ICCD) detector array. The effective linear dispersion was approximately 0.035 nm/pixel. Signal integration was performed by using delay times of 2.0, 4.0, 8.0, 12.0, 16.0, 24.0, 34.0, and 50.0 μs with respect to the initial laser pulse ($t = 0$) and corresponding total integration times of 2.0, 4.0, 4.0, 4.0, 8.0, 10.0, 16.0, and 150.0 μs , respectively. Signal integration was also performed at a delay time of 10.0 μs with an integration time of 10.0 μs . Measurements were taken for laser pulse energies of 175 and 330 mJ.

The laser pulse energies of 175 and 330 mJ are both significantly above the threshold required for laser-induced breakdown in ambient air (about 50 to 75 mJ per pulse). However, the lower energy level corresponds to the approximate pulse energy necessary to create a laser-induced plasma for 100 percent of laser shots. Hence a more robust plasma is produced with the higher pulse energies, which functions to uncouple the breakdown process from local matrix effects (e.g., aerosol particle loadings). It has been reported that increased laser-pulse energies produce a similar plasma with respect to temperature and free-electron density, but of a larger volume.^{11,20} The plasma-excitation temperatures varied from about 12 000 to 9000 K over delay times from 10 to 50 μs ,²⁵ and the characteristic plasma volume was equal to $2.5 \times 10^{-4} \text{ cm}^3$,²² as reported previously.

Particle source streams were generated with the use of both cross-flow and pneumatic-type nebulizers. Standard aqueous solutions of metals (10 mg/mL in 2 to 10% nitric acid solution) were nebulized (pure or diluted with de-ionized water) and introduced into an air carrier-gas flow stream at 30 °C, where the droplets subsequently dried to produce a dispersion of fine, solid particulates. Preliminary *ex situ* analysis of collected particles revealed sub-micron-sized particulates that contain metal oxides, although hydrated metal nitrates may be present. All species and particles, regardless of chemical state, are dissociated completely within the plasma. The mole fraction of water vapor was 0.002 in the final source stream. Precise calibration flows were generated with known total mass concentrations of metals that ranged from 350 to 17 500 micrograms per cubic meter ($\mu\text{g}/\text{m}^3$) of sample gas, which corresponds to a range from approximately 300 parts per billion to 15 parts per million on a mass

basis. For all elements, linear calibration curves of the atomic emission peak-to-base ratio as a function of mass concentration (based on system flow rates) were obtained with regression coefficients greater than 0.99. Precision was assessed by comparing the predicted mass concentration (calibration curve and LIBS signal) with the system mass flow rates for multiple experiments, which yielded an average relative standard deviation of less than 2%. In addition, the high degree of linearity of the calibration curves suggests negligible effects from self-absorption or self-reversal at the relatively high analyte concentration levels.

For a fixed metal concentration, ICCD detector delay time, and detector gate width, LIBS spectra were recorded and ensemble averaged for 900 laser pulses. This procedure was repeated in triplicate, and the three resulting spectra were averaged. Thus all reported spectra and data analysis correspond to an ensemble average of 2700 laser pulses. The spectral data were processed by calculating the integrated peak area of the atomic emission line, the baseline continuum emission intensity, and the root mean square (rms) noise of the continuum emission intensity in regions adjacent to the atomic emission line. The rms noise was calculated by fitting a linear curve to the continuum intensity over narrow spectral regions (20 to 30 pixels or about 0.8 nm) on both sides of the atomic emission line and then calculating the rms values based on the pixel-to-pixel variations from the linear fit. For each atomic emission line of interest, the final rms noise was taken as the average of these two values. The selected spectral regions were well suited to a linear fit, and the rms values calculated on each side of the atomic emission lines were in excellent agreement for all cases. The reported signal-to-noise ratio (SNR) is the absolute intensity of the integrated peak area divided by the absolute value of the rms noise times the width of the peak area:

$$\text{SNR} = \frac{\text{integrated peak area}}{(\text{RMS noise})(\text{peakwidth})} \quad (1)$$

The limit of detection (LOD) was based on a limiting SNR value of 3 and was evaluated by using the corresponding LIBS signal (integrated peak area) and the measured rms noise at a known analyte concentration:

$$\text{LOD} = \frac{3x}{(\text{SNR} @ x)} \quad (2)$$

where x is a known analyte concentration and the SNR is evaluated per Eq. 1 at the known analyte concentration. All experiments were performed over a range of analyte concentrations characterized by a linear LIBS signal response function. It is noted that the optimal limits of spectral integration of the atomic emission lines, with respect to the overall signal-to-noise ratio, are not the entire peak area as used here. Voigtman calculates an optimum integration window equal to approximately ± 1.39 times the half-width half-maximum (HWHM) of the analyte peak for a Lorentzian line shape.²⁶ Such an analysis would enhance our reported limits of detection but would not change the relative comparisons between the different detector gates and elements.

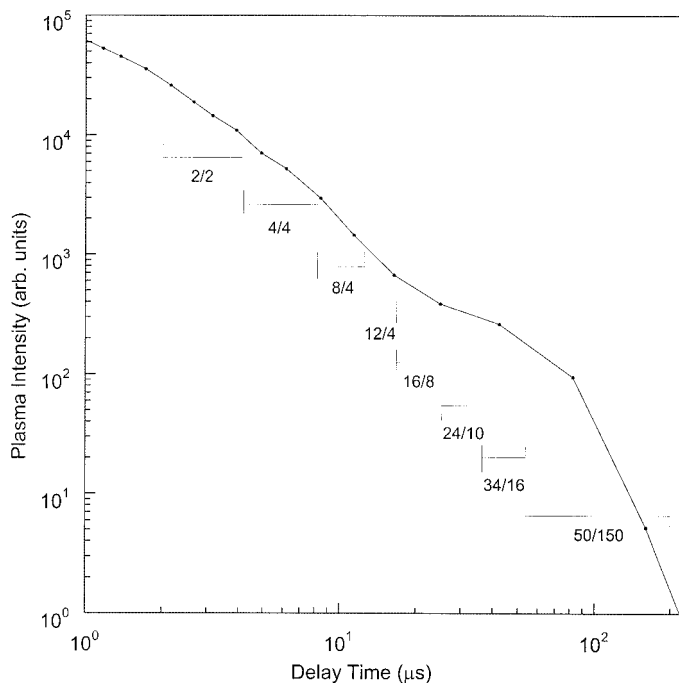


FIG. 2. Integrated plasma emission intensity in the 233.5 to 266.5 nm spectral region as a function of delay time from the plasma-initiating laser pulse. The investigated detector gates are indicated corresponding to the delay and width (delay/width) in microseconds.

RESULTS AND DISCUSSION

The temporal plasma intensity, as measured by the collected plasma emission with the optical system described above, was recorded at two spectral locations, namely, from 233.5 to 266.5 nm and from 375.4 to 403.8 nm. In each spectral region, the reported plasma emission intensity corresponds to the integrated intensity (continuum and emission lines) over each spectral band. The peak plasma emission intensity corresponded to the trailing edge of the incident laser pulse; hence the plasma is formed on a nanosecond time scale coincident with the initiating laser pulse. The plasma intensity decayed by over one order of magnitude 1 μ s after the incident laser pulse ($t = 0$), which, as discussed above, is the approximate time required to establish local thermodynamic equilibrium within the plasma. Beginning 1 μ s after the laser pulse, the plasma emission intensity in the 233.5 to 266.5 nm spectral region is presented in Fig. 2 as a function of delay time. The detector gate width was increased with increasing delay time as described above. The plasma emission intensity decays by slightly more than three orders of magnitude from a delay time of 1 μ s to a delay of 100 μ s. Similar temporal behavior was recorded for the 375.4 to 403.8 nm spectral region.

The distinct temporal detection windows used for the current optimization are shown in Fig. 2. The first window corresponds to a 2 μ s delay with respect to the laser pulse and a 2 μ s signal integration gate width (designated 2/2 μ s). With the use of this nomenclature, the remaining windows are 4/4, 8/4, 12/4, 16/8, 24/10, 34/16, and 50/150 μ s. The authors are aware of no published LIBS work that considers the analysis of metal-based aerosols in the temporal region 50 to 200 μ s after the incident laser pulse. The lack of LIBS data in this temporal region

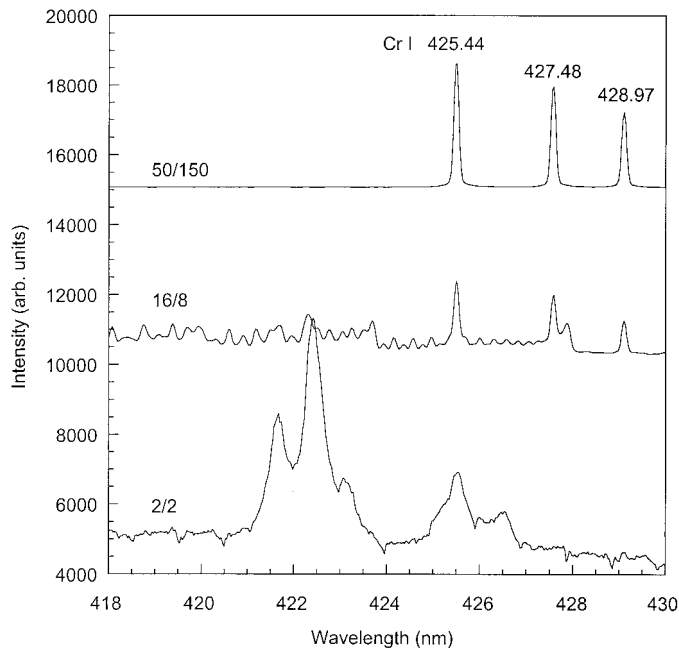


FIG. 3. LIBS spectra showing the Cr I atomic emission lines for the 2/2, 16/8, and 50/150 μ s signal integration gates. The chromium concentration is 3500 μ g/m³. All spectra have the same scale and have been shifted vertically for clarity.

may be due to the high degree of decay in the plasma emission, in which it may be concluded that the plasma has essentially dissipated. This is especially true when examining the plasma emission intensity with a fixed integration gate width. In this study, the average plasma emission intensity decays by more than a factor of ten between the 2/2 and the 12/4 μ s windows, as well as between the 12/4 and 50/150 μ s windows. However, by increasing the detector gate width concurrently with the detector delay time, comparable plasma emission signal levels may be obtained. The rate of plasma emission decay as a function of delay time increases as the wavelength increases; hence additional detector gain is beneficial for working further in the red. Nonetheless, with respect to overall signal strengths, practical LIBS measurements can be performed for each of the selected temporal integration windows.

The LIBS spectra that correspond to the Cr I atomic emission lines at 425.44, 427.48, and 428.97 nm are presented in Fig. 3, corresponding to detector gates of 2/2, 16/8, and 50/150 μ s. The chromium concentration was 3500 μ g/m³ for all three spectra. The significant feature of Fig. 3 is the very long induction time for the chromium emission at these wavelengths, with atomic emission becoming visible only after tens of microseconds following the laser pulse. Table I shows the optimal SNR values at both low (175 mJ) and high (330 mJ) laser pulse energy for the two most pronounced chromium emission lines, namely, 425.4 and 429.0 nm. The low-energy SNR was calculated as 158, and the high-energy SNR was calculated as 311 for the 425.44 nm line. For the 428.97 nm line, the low-energy and high-energy SNR values were 225 and 303, respectively. Clearly, higher pulse energy yields a larger SNR for chromium atomic emission. As illustrated in Table I, this trend was observed for all of

TABLE I. Optimal signal-to-noise (SNR) ratios for various metal emission lines for low energy (175 mJ) and high energy (330 mJ) laser pulses. The detector gate (delay/width) corresponds to the optimal SNR ratio.

Element/line (nm)	SNR (175 mJ) (Optimal gate, μ s)	SNR (330 mJ) (Optimal gate)	SNR ratio (330 mJ/175 mJ)
As 228.81 I	105 (4/4)	133 (8/4)	1.3
Be 234.86 I	23 (12/4)	28 (12/4)	1.2
Be 313.1 II	96 (4/4)	95 (12/4)	1.0
Cd 226.50 II	111 (4/4)	180 (8/4)	1.6
Cd 228.80 I	69 (8/4)	87 (12/4)	1.3
Cr 425.44 I	158 (34/16)	311 (50/150)	2.0
Cr 428.97 I	225 (34/16)	303 (50/150)	1.3
Hg 253.65 I	55 (8/4)	47 (12/4)	0.85
Pb 405.78 I	54 (24/10)	56 (50/150)	1.1

the investigated emission lines with the exception of mercury. Limits of detection were subsequently calculated by using only the high-energy SNR for all species. Table II presents four limit of detection (LOD) values for each emission line. The first is the optimal LOD value with respect to temporal gating, as calculated from the optimal SNR. Limits of detection are also shown for relatively short (12/4 μ s), intermediate (24/10 μ s), and long (50/150 μ s) detector gates. The optimal limit of detection for chromium is 30 μ g/m³ with the 425.44 nm line and 40 μ g/m³ with the 428.97 nm line, corresponding to the 50/150 μ s detector gate.

The temporal behavior of the SNR for the 425.44 nm chromium emission line is shown in Figs. 4 and 5 for the 330 and 175 mJ pulse energies, respectively. For clarity, the SNR value is normalized with respect to the optimal SNR value, denoted as 100%. Both plots show similar behavior, with a low SNR at short to intermediate delay times, followed by a rapid increase to a maximum SNR value at delay times from 34 to 50 μ s. The only significant difference with pulse energy is that the SNR peaks at a 34 μ s delay for 175 mJ pulse energy, while the SNR

TABLE II. Limit of detection (LOD) values for various metal emission lines for the optimal detector gates (see Table I), as well as for detector gates (delay/width) of 12/4, 24/10, and 50/150 μ s. The average relative standard deviation is 8% for the optimal LOD values.

Element/line (nm)	Optimal LOD (μ g/m ³)	LOD at 12/4 (μ g/m ³)	LOD at 24/10 (μ g/m ³)	LOD at 50/150 (μ g/m ³)
As 228.81	400	460	940	2500
Be 234.86	40	40 ^a	50	60
Be 313.1	10	10 ^a	20	730
Cd 226.50	60	80	270	690
Cd 228.80	120	120 ^a	220	360
Cr 425.44	30	1500	550	30 ^a
Cr 428.97	40	1100	210	40 ^a
Hg 253.65	230	230 ^a	410	1470
Pb 405.78	190	4200	600	190 ^a

^a Indicates the optimal detector gate.

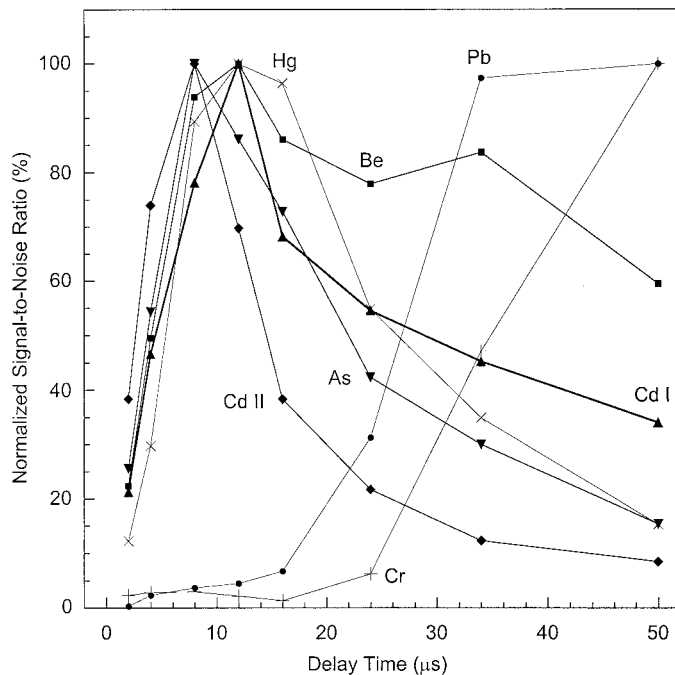


FIG. 4. The signal-to-noise ratios (SNR) as a function of plasma decay time with respect to the plasma-initiating pulse for the various detector gates depicted in Fig. 2. The laser pulse energy is 330 mJ. The SNR values have been normalized with respect to the optimal value.

peaks at a 50 μ s delay for the 330 mJ energy. This follows from the fact that the lower pulse energy results in a smaller plasma volume, which is expected to decay faster due to the increased surface-to-volume ratio. As a consequence, the temporal decay process is shifted to shorter times with decreased pulse energy. Although not

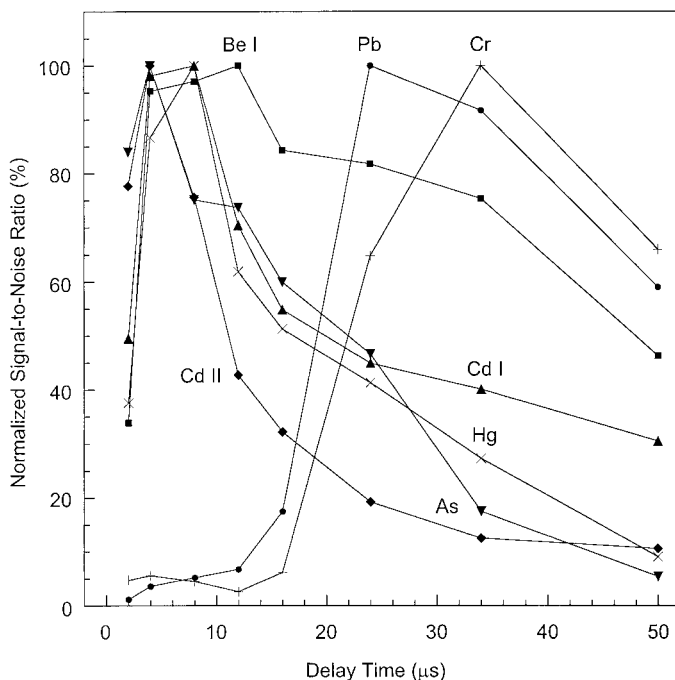


FIG. 5. The signal-to-noise ratios (SNR) as a function of plasma decay time with respect to the plasma-initiating pulse for the various detector gates depicted in Fig. 2. The laser pulse energy is 175 mJ. The SNR values have been normalized with respect to the optimal value.

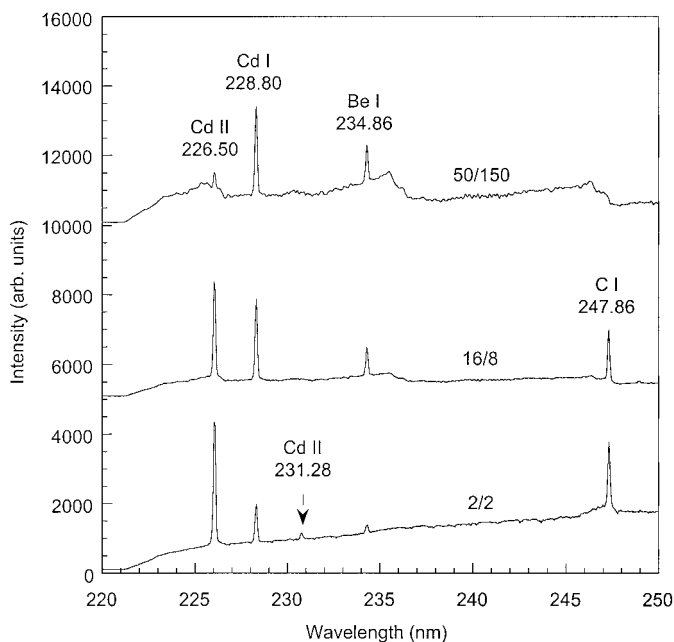


Fig. 6. LIBS spectra showing the Cd I, Cd II, and Be I atomic emission lines for the 2/2, 16/8, and 50/150 μs signal integration gates. The cadmium concentration is 3500 $\mu\text{g}/\text{m}^3$ and the beryllium concentration is 350 $\mu\text{g}/\text{m}^3$ for all spectra. All spectra have the same scale and have been shifted vertically for clarity.

shown in Figs. 4 and 5, the temporal behavior of the SNR for the 428.97 nm emission line was very similar to that of the 425.44 nm line at both energy levels. The SNR was, however, nominally 25–50% lower at each time step for the 428.97 nm peak, which is consistent with the greater peak height of the 425.44 nm emission line, as observed in Fig. 3. The optimal ratio of the integrated peak intensity to the baseline intensity, the signal-to-baseline ratio (SBR), was 558 for the 425.44 nm peak as compared to 411 for the 428.97 nm peak, corresponding to the respective SNR and SBR values can be significant in that the temporal behavior of the SNR and SBR values, while similar, are not always coincident. For example, Singh et al. noted more than a factor of two difference between the relative changes in the SNR and SBR when analyzing gas matrix effects in a LIBS study of metal hydrides.¹⁹ The signal-to-noise ratio is the correct ratio for signal optimization, although this distinction between the signal-to-noise ratio and the signal-to-baseline ratio is at times overlooked when optimizing the LIBS signal for detection and analysis of a given analyte.

The LIBS spectra for cadmium are presented in Fig. 6 over the spectral region that contains the Cd I line at 228.80 nm and the Cd II lines at 226.50 and 231.28 nm. The spectra correspond to cadmium present at a concentration of 3500 $\mu\text{g}/\text{m}^3$ for all three detector gates. Both the Cd II line at 226.50 nm and the Cd I line at 228.80 nm are pronounced at all delay times; hence both emission lines were analyzed. For the 226.50 nm line, the optimal SNR was 111 and 180 for the 175 and 330 mJ pulse energies, respectively. For the 228.80 nm line, the SNR values were 69 and 87 for the low and high pulse energies, respectively. As with chromium, the higher pulse energy produces a higher SNR. As seen in Fig. 4,

the 226.50 nm emission line exhibits a maximum SNR in the 8/4 μs detector gate, while the 228.80 nm line is maximized with the 12/4 μs gate. The limit of detection for cadmium is 60 $\mu\text{g}/\text{m}^3$, or about 50 ppb by mass, based on the 226.50 nm line, the 8/4 μs detector gate, and 330 mJ pulse energy.

The temporal behavior of cadmium contrasts with chromium emission, which yields a maximum SNR for the relatively long detector gate of 50/150 μs . As discussed below, the six metals may be divided into two groups based on the temporal emission characteristics, specifically, those that exhibit a relatively short optimal delay (As, Be, Cd, and Hg) and those that exhibit an optimal SNR at long delay times (Cr and Pb).

As with cadmium, beryllium exhibits strong atomic emission that corresponds to both neutral and ionic states. Spectra containing the Be I emission line at 234.86 nm are also presented in Fig. 6 for three distinct detector gates. Beryllium data were recorded at a concentration of 350 $\mu\text{g}/\text{m}^3$ due to the relatively strong atomic emission of this element. The 313.1 nm Be II doublet was also analyzed and yielded results similar to the 234.86 nm line except that the SNR signal decreased more rapidly with time, as expected for the ionized Be II line. The optimal SNR value was 28 for the 234.86 nm line and 95 for the 313.0 nm Be II doublet, both corresponding to the 12/4 μs detector gate and 330 mJ pulse energy. The optimal LOD values are presented in Table II for both beryllium emission lines. Unlike chromium and cadmium, as discussed above, the maximum SNR of beryllium did not correspond with the maximum signal-to-baseline ratio. The SBR for the 234.86 nm line reached a maximum value for the 24/10 μs gate, at which point the SNR was 22% less than the maximum SNR recorded for the 12/4 μs detector gate.

Mercury spectra corresponding to the 253.65 nm Hg I emission line were recorded at a concentration of 3500 $\mu\text{g}/\text{m}^3$. Unique with respect to the other metals investigated, the 253.65 nm mercury line exhibited a higher SNR with the 175 mJ pulse energy as compared with the 330 mJ pulse energy. A recent, more detailed investigation of mercury revealed a strong influence of oxygen on the 253.65 nm mercury emission line.²⁵ Specifically, oxygen species are dissociated initially within the plasma and then recombine at intermediate to long delay times. The recombination of atomic oxygen is coincident with a reduction in 253.65 nm emission. Therefore, temporal changes in the plasma processes, including atomic recombination, are manifest in the observed mercury signal enhancement with reduced pulse energy. Because simultaneous detection of all metal species is a motivating factor for this study, mercury was optimized by using the 330 mJ pulse energy, which yielded an optimal SNR of 47 with the use of the 12/4 μs detector gate. The corresponding limit of detection is 230 $\mu\text{g}/\text{m}^3$. Repeated experiments that used a pure nitrogen coflow yielded an enhanced limit of detection of 25 $\mu\text{g}/\text{m}^3$, or about 22 ppb by mass, consistent with the earlier findings discussed above.²⁵ Mercury, like beryllium and cadmium, is characterized by an optimal SNR at moderate delay times, followed by a rapid decrease at longer delay times as illustrated in Figs. 4 and 5.

The more intense 405.78 nm Pb I emission line was

investigated in detail, although preliminary data were recorded for the 363.96 and 367.15 nm Pb I emission lines. The lead emission was characterized by a long induction time, with no significant atomic emission observed until a delay greater than 12 μ s, similar to the effects observed with chromium. The SNR was 56 for the 330 mJ pulse energy and the 50/150 μ s detector gate, with a corresponding limit of detection equal to 190 μ g/m³. This LIBS-based lead detection limit is comparable to a value of about 150 μ g/m³ reported by Neuhauser et al., corresponding to a somewhat shortened detection window and a laser pulse energy of about 50 mJ/pulse.²¹

Arsenic was investigated with the use of the 228.81 nm emission line. Due to the low emission intensity of this line, arsenic data were recorded at a nominal concentration of 17 500 μ g/m³. Similar to beryllium, cadmium, and mercury, arsenic exhibited the strongest emission at short delay times and was characterized by a rapid decrease in signal at intermediate to long delay times. The optimal SNR was 133 with the use of the 8/4 μ s detector gate, which yields a limit of detection value of 400 μ g/m³. It is noted that the 228.81 nm arsenic emission line is coincident with the 228.80 nm cadmium line. Cadmium spectral interference is readily identified by the presence of the additional cadmium lines discussed above. Additional arsenic emission lines are present at 189.04 and 193.76; however, limited optical system response at these short UV wavelengths may limit accessibility.

The six metals investigated here may be divided into two groups based on the temporal emission characteristics, specifically, those that exhibit a relatively shorter optimal delay (As, Be, Cd, and Hg), and those that exhibit an optimal SNR at longer delay times (Cr and Pb). These temporal characteristics may be related to the temporal decay in plasma temperature and the associated ionic states and energy levels of the respective transitions. Ionized atoms are limited to early times within the plasma and rapidly form neutral atoms via electron recapture at short to intermediate decay times.¹¹ The temporal behavior of the Be II and Cd II emission lines is consistent with this transition to neutral atoms. For some neutral atoms, relatively low upper state energy levels result in stable upper state populations for the high plasma temperatures corresponding to short decay times, which results in relatively low atomic emission during this period. This is consistent with the chromium and lead temporal data. The upper energy levels are 23 499 and 23 305 cm^{-1} for the chromium 425.44 and 428.97 nm lines, respectively, and 35 387 cm^{-1} for the 405.78-nm lead line. In contrast, the elements exhibiting optimal atomic emission at relatively short delay times have significantly higher upper energy levels that decay rapidly as the plasma cools, namely, 54 605 cm^{-1} for the 228.82 nm arsenic line, 42 565 cm^{-1} for the 234.86 nm beryllium line, and 43 692 cm^{-1} for the 226.5 nm cadmium line. As a result, these elements are optimized at shorter decay times. Mercury is an anomaly: the upper energy level of the 253.65 nm mercury line is 39 412 cm^{-1} ; however, the temporal characteristics of mercury are significantly influenced by oxygen as discussed above. Although mercury may exist as a vapor at elevated temperatures (e.g., combustor flue gases), the dissociation and subsequent excitation of mer-

cury in the laser-induced plasma are not expected to be influenced by the chemical or physical state, whether vapor phase or particulate bound.

The detection limits for beryllium, cadmium, and chromium reported in Table II are consistent with new U.S. EPA MACT standards for emissions from existing hazardous waste incinerators. The MACT standards are defined for groups of metals: the emission standards for the semi-volatile metals Pb and Cd are 240 μ g per dry standard cubic meter, 130 μ g per dry standard cubic meter for mercury, and for the low-volatility metals As, Be, and Cr, are 97 μ g per dry standard cubic meter. For new incinerators, the MACT emission standards are reduced to 24 and 45 μ g per dry standard cubic meter for the semi-volatile metals and mercury, respectively. For real-time monitoring applications, it is noted that analyte detection under actual operating conditions may differ significantly from laboratory assessment. The complexity of multimetals monitoring, including LIBS-based analysis, in actual process waste streams was demonstrated in a recent U.S. DOE and EPA cosponsored test program.²⁷ Therefore, while the detection limits in Table II provide a relative assessment of the LIBS technique, care must be used for the estimation of practical limits of quantitation under actual process conditions. These comments notwithstanding, the results of the current investigation demonstrate that the LIBS technique is a viable candidate for on-line analysis and detection of toxic metal emissions, although improvements must still be made in the detection limits to achieve true *in situ* multimetals monitoring capability. It is noted that the Table II LOD values correspond to ensemble averaging of LIBS spectra and the nonoptimal use of the total integrated emission line intensity, as performed in this work. Improvements are expected with the use of optimal signal processing. Furthermore, due to the particulate nature of metal species in most emissions waste streams, considerable improvements in the lower detection limits can be realized through discrete particle detection and conditional data analysis.^{6,23}

Additional comments are offered with respect to the gas matrices investigated in the current work. The use of a nitrogen carrier gas yielded comparable or modest increases in signal-to-noise ratios as compared to an air carrier gas for the range of experimental conditions investigated. A noted exception is mercury, which is characterized by significant suppression of the 253.65 nm emission line with the presence of oxygen-containing species. Hence nitrogen should be considered as a carrier gas when nebulizing aqueous solutions or particle suspensions for LIBS analysis. For the LIBS-based analysis of metal particulates from ambient air or gaseous emissions from waste streams, the use of a nitrogen coflow may enhance sensitivity.

CONCLUSION

The LIBS technique is applicable for the detection and analysis of the RCRA-listed toxic metals arsenic, beryllium, cadmium, chromium, lead, and mercury. Because the laser-induced plasma is a transient process, in which the emission intensity decays with a time scale on the order of 100 μ s, temporal gating of the detection system

is necessary for the optimal detection of a given analyte. Historically, much of the LIBS-based research for the analysis of metal species has employed signal gating over a temporal region between several microseconds after the plasma-initiating laser pulse to tens of microseconds after plasma initiation. In this short to intermediate time regime, both the plasma emission intensity and the atomic emission intensity are strong, although the resulting signal-to-noise ratios may not be optimal. For the current experimental conditions, it is concluded that the relatively short delay time of 12 μs is optimal for the detection of arsenic, beryllium, cadmium, and mercury, while a longer delay time of 50 μs is optimal for the detection of chromium and lead. The reduced atomic emission intensity at relatively long delay times is compensated for by the use of long detector gate widths. Overall, as modern echelle spectrometer systems become available, the simultaneous detection of multiple metal species becomes feasible. However, optimization of often-disparate temporal atomic emission profiles must be considered and may be further coupled with expected relative concentrations of the various metals during system implementation.

ACKNOWLEDGMENTS

This work was supported in part by the U.S. DOE Office of Technology Development/CMST-CP and by the U.S. DOD Office of Munitions/JS DTO, both directly and through subcontracts with Sandia National Laboratories.

1. Revised standards for hazardous waste combustors, performance specification 10. *Fed. Regs.* **61**, 17357 (1996).
2. N. B. French and M. Durham, *Proc. International Conf. On Incineration and Thermal Treatment Technologies*, University of California, 399 (1996).
3. D. Nore, A. M. Gomes, J. Bacri, and J. Cabe, *Spectrochim. Acta, Part B* **48**, 1411 (1993).

4. P. P. Woskov, D. Y. Rhee, P. Thomas, D. R. Cohn, J. E. Surma, and C. H. Titus, *Rev. Sci. Instrum.* **67**, 3700 (1996).
5. M. D. Seltzer, *J. Air Waste Manage. Assoc.* **50**, 1010 (2000).
6. D. W. Hahn, W. L. Flower, and K. R. Hencken, *Appl. Spectrosc.* **51**, 1836 (1997).
7. H. Zhang, F. Y. Yueh, and J. P. Singh, *Appl. Opt.* **8**, 1459 (1999).
8. R. E. Neuhauser, U. Panne, and R. Niessner, *Anal. Chim. Acta* **392**, 47 (1999).
9. S. G. Buckley, H. A. Johnsen, K. R. Hencken, and D. W. Hahn, *Waste Manage.* **20**, 455 (2000).
10. W. L. Clevenger, B. W. Smith, and J. D. Winefordner, *Crit. Rev. Anal. Chem.* **27**, 1 (1997).
11. L. J. Radziemski, T. R. Loree, D. A. Cremers, and N. M. Hoffman, *Anal. Chem.* **55**, 1246 (1983).
12. M. Essien, L. J. Radziemski, and J. J. Sneddon, *J. Anal. At. Spectrom.* **3**, 985 (1988).
13. M. Casini, M. A. Harith, V. Palleschi, A. Savletti, D. P. Singh, and M. Vaselli, *Laser Part. Beams* **9**, 633 (1991).
14. C. Lazzari, M. DeRosa, S. Rastelli, A. Ciucci, V. Palleschi, and A. Salvetti, *Laser Part. Beams* **12**, 525 (1994).
15. I. Schechter, *Anal. Sci. Technol.* (J. Korean Soc. Anal. Sciences) **8**, 779 (1995).
16. W. L. Flower, L. W. Peng, M. P. Bonin, N. B. French, H. A. Johnsen, D. K. Ottesen, R. F. Renzi, and L. V. Westbrook, *Fuel Process. Technol.* **39**, 277 (1994).
17. H. Zhang, J. P. Singh, F. Y. Yueh, and R. L. Cook, *Appl. Spectrosc.* **49**, 1617 (1995).
18. J. P. Singh, F. Y. Yueh, H. S. Zhang, and R. L. Cook, *Process Contr. Qual.* **10**, 247 (1997).
19. J. P. Singh, H. Zhang, F. Y. Yueh, and K. P. Carney, *Appl. Spectrosc.* **50**, 764 (1996).
20. S. Yalcin, D. R. Crosley, G. P. Smith, and G. W. Faris, *Hazard. Waste Hazard.* **13**, 51 (1996).
21. R. E. Neuhauser, U. Panne, R. Niessner, G. A. Petrucci, P. Cavalli, and N. Omenetto, *Anal. Chim. Acta* **346**, 37 (1997).
22. D. W. Hahn, *Appl. Phys. Lett.* **72**, 2960 (1998).
23. D. W. Hahn and M. M. Lunden, *Aerosol Sci. Technol.* **33**, 30 (2000).
24. M. Milan, J. M. Vadillo, and J. J. Laserna, *J. Anal. At. Spectrom.* **12**, 441 (1997).
25. R. L. Gleason and D. W. Hahn, *Spectrochim. Acta, Part B* **56**, 419 (2001).
26. E. Voigtman, *Appl. Spectrosc.* **45**, 237 (1991).
27. P. M. Lemieux, J. V. Ryan, N. B. French, W. J. Haas, S. J. Priebe, and D. B. Burns, *Waste Manage.* **18**, 385 (1998).